2017

Proteolytic degradation of regulator of G protein signaling 2 facilitates temporal regulation of Gq/11 signaling and vascular contraction

Stanley M. Kanai
Washington University School of Medicine in St. Louis

Alethia J. Edwards
Drexel University College of Medicine

Joel G. Rurik
Washington University School of Medicine in St. Louis

Patrick Osei-Owusu
Drexel University College of Medicine

Kendall J. Blumer
Washington University School of Medicine in St. Louis

Proteolytic degradation of regulator of G protein signaling 2 facilitates temporal regulation of $G_{q/11}$ signaling and vascular contraction

Received for publication, May 16, 2017, and in revised form, September 18, 2017 Published, Papers in Press, October 3, 2017, DOI 10.1074/jbc.M117.797134

Stanley M. Kanai[‡], Alethia J. Edwards[§], Joel G. Rurik[‡], Patrick Osei-Owusu[§], and Kendall J. Blumer[‡1]

From the [‡]Department of Cell Biology and Physiology, Washington University School of Medicine, St. Louis, Missouri 63110 and [§]Department of Pharmacology and Physiology, Drexel University College of Medicine, Philadelphia, Pennsylvania 19102

Edited by Henrik G. Dohlman

Regulator of G protein signaling 2 (RGS2) controls signaling by receptors coupled to the $G_{q/11}$ class heterotrimeric G proteins. RGS2 deficiency causes several phenotypes in mice and occurs in several diseases, including hypertension in which a proteolytically unstable RGS2 mutant has been reported. However, the mechanisms and functions of RGS2 proteolysis remain poorly understood. Here we addressed these questions by identifying degradation signals in RGS2, and studying dynamic regulation of $G_{q/11}$-evoked Ca^{2+} signaling and vascular contraction. We identified a novel bipartite degradation signal in the N-terminal domain of RGS2. Mutations disrupting this signal blunted proteolytic degradation downstream of E3 ubiquitin ligase binding to RGS2. Analysis of RGS2 mutants proteolyzed at various rates and the effects of proteasome inhibition indicated that proteolytic degradation controls agonist efficacy by setting RGS2 protein expression levels, and affecting the rate at which cells regain agonist responsiveness as synthesis of RGS2 stops. Analyzing contraction of mesenteric resistance arteries supported the biological relevance of this mechanism. Because RGS2 mRNA expression often is strikingly and transiently up-regulated and then down-regulated upon cell stimulation, our findings indicate that proteolytic degradation tightly couples RGS2 transcription, protein levels, and function. Together these mechanisms provide tight temporal control of $G_{q/11}$-coupled receptor signaling in the cardiovascular, immune, and nervous systems.

Signal transduction by G protein–coupled receptors (GPCRs)[2] in mammalian cells is regulated by diverse mechanisms that determine agonist response amplitude (efficacy), kinetics, desensitization, and resensitization, thereby providing novel drug targets to modulate GPCR signaling in many diseases (1). Among these regulatory mechanisms, those mediated by the regulator of G protein signaling (RGS) family of proteins are crucial as indicated by diverse phenotypes of mice lacking certain RGS proteins or expressing RGS-insensitive G protein mutants (2, 3) and humans bearing mutations in RGS-encoding genes (4–6). These phenotypes are thought to occur because many RGS proteins regulate the amplitude and kinetics of GPCR signaling by functioning as GTPase-activating proteins (GAPs) for G protein α-subunits (7), and because certain RGS proteins also affect cell signaling by GAP-independent mechanisms (8).

Among >30 RGS proteins encoded by the human genome, RGS2 is of particular interest. RGS2 is a GAP that acts preferentially toward $G_{q/11}$ class α-subunits relative to $G_{i/o}$ α-subunits (9–12), and has several GAP-independent functions (8, 13, 14). RGS2 is expressed in many organs, tissues, and cell types where it participates in diverse physiological and disease processes including T cell activation (15), blood pressure regulation (16–20), cardiac hypertrophy and heart failure (21–23), renal hemodynamics (20), anxiety (15, 24), and certain cancers (25).

A key emerging concept is that physiological and disease processes are strikingly sensitive even to modest changes in RGS2 function or expression level. For example, loss of just one RGS2 allele is sufficient to elevate blood pressure in mice (16), rare missense mutations that reduce RGS2 protein expression are associated with hypertension in humans (5, 6), and RGS2 down-regulation occurs in human hypertension (26). Furthermore, in several tissues and cell systems RGS2 mRNA expression is strikingly and transiently up- and then down-regulated in response to cell stimulation (11, 27–34), potentially serving as an inducible feedback loop that attenuates or desensitizes GPCR signaling.

Such evidence has motivated efforts to identify mechanisms that regulate RGS2 expression or function, which could provide new insight into disease pathogenesis or novel targets for therapeutic development. Among such mechanisms, proteolytic degradation of RGS2 may be particularly important. RGS2 protein half-life is short (~30 min) because of ubiquitin- and proteasome-mediated proteolysis (35–37). Targeting this process has therapeutic potential because cardiotonic steroids such as digoxin inhibit RGS2 degradation and protect in mouse models against cardiac injury in an RGS2-dependent manner (38).

Mechanisms that mediate proteolytic degradation of RGS2 are complex. One mechanism is the acetylated N-end (Ac/N)

These studies were supported by National Institutes of Health Grants GM044592 and HL075632 (to K. J. B.) and American Heart Association Grant 16SDG27260276 (to P. O.-O.). The authors declare that they have no conflicts of interest with the contents of this article. The content is solely the responsibility of the authors and does not necessarily represent the official views of the National Institutes of Health.

[1] To whom correspondence should be addressed: Box 8228, 660 S. Euclid Ave., St. Louis, MO 63110. Tel.: 314-362-1668; Fax: 314-362-7463; E-mail: kblumer@wustl.edu.

[2] The abbreviations used are: GPCR, G protein–coupled receptor; RGS, regulator of G protein signaling; GAP, GTPase-activating protein; Ac/N, acetylated N-end; CHX, cycloheximide; MAs, mesenteric resistance arteries; EFS, electrical field stimulation; PSS, poly(styrenesulfonate); AUC, area under the curve.

rule pathway involving the identity of the amino acid at position 2 in RGS2, the N-recognin TEB4 (MARCH6), and the N-terminal acetylase Naa60 (37). However, other mechanisms have been implicated because RGS2 degradation also requires a ubiquitin E3 ligase complex (CUL4B/DDB1/FBXO44) unlinked to the N-end rule pathway (36). RGS2 degradation is a regulated process, as indicated by the inhibitory effects of cardiotonic steroids (38, 39), protein kinase C (PKC) activators (40), or a cGMP-dependent protein kinase (cGK) inhibitor (41). Whether such effects occur by targeting recognition of RGS2 by the Ac/N-end rule and/or CUL4B/DDB1/FBXO44 pathways is unknown.

Less well-understood is how proteolytic degradation of RGS2 affects GPCR signaling. A rapidly proteolyzed hypertension-associated RGS2 mutant (Q2L) exhibits reduced function (35), but whether this effect occurs by proteolytic degradation or other mechanisms has not been established. Similarly, although knock down of Ac/N-end rule components blunts RGS2 proteolysis and enhances inhibition of G_q-mediated ERK activation (37), whether this effect on cell signaling occurs specifically by inhibiting proteolytic degradation of RGS2 as opposed to other molecules is unclear. Moreover, whereas knockdown of the CUL4B/DBB1/FBXO44 complex inhibits RGS2 degradation (36), its effect on GPCR signaling was not investigated. Lastly, whether RGS2 proteolysis regulates GPCR signaling amplitude, kinetics, desensitization, or resensitization has not been studied.

Here our goals were to determine how RGS2 is targeted for ubiquitin- and proteasome-mediated degradation and to establish how $G_{q/11}$-mediated GPCR signaling is regulated by RGS2 proteolysis. Rather than knocking down components of the N-end rule or other pathways, which could have pleiotropic effects on cell signaling, we have used a structure-function approach to identify and characterize degradation signals in RGS2. By analyzing RGS2 mutants that degrade faster or more slowly than the wild-type protein and assessing the impact of proteasome inhibition, we have identified novel degradation signals and provided direct evidence indicating that proteolytic degradation of RGS2 regulates the amplitude and dynamics of $G_{q/11}$-mediated GPCR signaling.

Results

RGS2 degradation requires a novel N-terminal bipartite motif

Because N-terminal acetylation and the identity of the amino acid at position 2 in RGS2 are the only features of this protein shown thus far to affect proteolytic degradation, our first goal was to conduct a more comprehensive identification of motifs or domains that are necessary and sufficient for RGS2 proteolysis. Our approach was guided by the domain structure of RGS2, a 211-residue protein containing an ~80-residue N-terminal region, followed by the RGS domain that is necessary and sufficient for GAP activity, and a short C-terminal tail (Fig. 1*A*). We began by studying the degradation rates of RGS2 translated from four previously identified alternative in-frame initiation sites at methionine 1, 5, 16, and 33 (Met-1, Met-5, Met-16, Met-33) (Fig. 1, *A* and *B*) (31, 42–44) and to explore the role of the N-terminal region. Which of these alternative translation

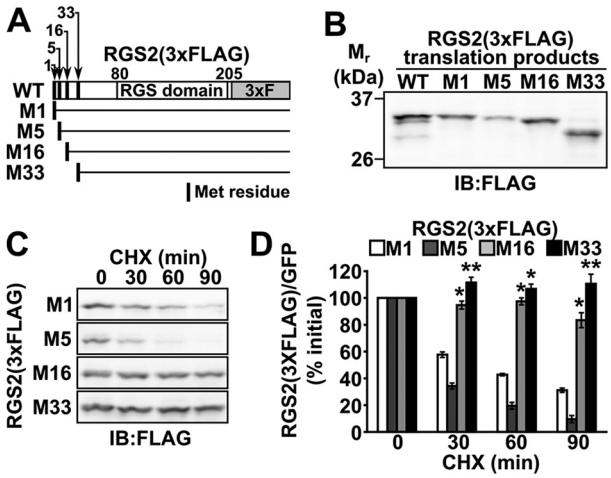

Figure 1. RGS2 synthesized from alternative translation initiation sites is degraded at different rates. *A*, domain structure of RGS2 produced by alternative translation initiation. The RGS domain is flanked by an N-terminal region that contains multiple translation start codons numbered by their position in the longest open reading frame, as indicated by solid vertical *bars* and *arrows*. Single translation products initiated from a given methionine residue were produced by changing all other alternative methionine codons to leucine codons, and tagging them at their C terminus with the 3xFLAG epitope. *B*, RGS2(3xFLAG) produced in HEK 293 cells by translation initiated from single alternative methionine codons. *C*, proteolytic degradation of RGS2(3xFLAG) initiated at single alternative translation start sites. Transfected HEK 293 cells expressing RGS2(3xFLAG) initiated at the indicated methionine codons were treated with cycloheximide (CHX) and analyzed at the indicated time points by immunoblotting to detect RGS2(3xFLAG) remaining. *D*, quantification of RGS2(3xFLAG) protein levels detected by immunoblotting following addition of CHX. *Error bars* denote S.E. *, $p < 0.05$; **, $p < 0.01$ *versus* Met-1–RGS2(3xFLAG). Data shown are representative of three or more independent experiments.

products are expressed endogenously in cells or tissues remains unclear because of low expression, rapid degradation, or limitations of antibodies used for detection. Regardless, the N-end rule machinery is predicted to recognize each of these alternative translation products based on the identity of the amino acid residue immediately following the initiating methionine (*i.e.* Gln-2, Phe-6, Asp-17, Lys-34) (45). To study RGS2 degradation, we tagged the protein at its C terminus with three copies of the FLAG epitope (RGS2(3xFLAG)), which preserves function (see below). To simplify analysis, single translation products initiated only at methionine 1, 5, 16, or 33 were produced by changing other alternative in-frame start sites to leucine codons. Degradation rates of RGS2(3xFLAG) initiated at single translation start sites were determined by quantitative immunoblotting of transfected HEK 293 cell lysates harvested over time after inhibiting new protein synthesis with cycloheximide (CHX) (Fig. 1*C*), and by pulse-chase labeling experiments.[3] Results indicated that RGS2 initiated at methionine 1 or 5 was degraded more rapidly than RGS2 initiated at methionine 16 or 33 (Fig. 1, *C* and *D*), suggesting that a motif between methionine 5 and 16 promotes RGS2 degradation.

To test this hypothesis, we generated small internal deletions in RGS2(3xFLAG) initiated at methionine 1 (Met-1–RGS2(3xFLAG)) (Fig. 2*A*) and analyzed their effects on degradation rates following CHX treatment. Deletion of residues 5–9 impaired RGS2 degradation whereas removing residues 8–12

[3] S. M. Kanai and K. J. Blumer, unpublished data.

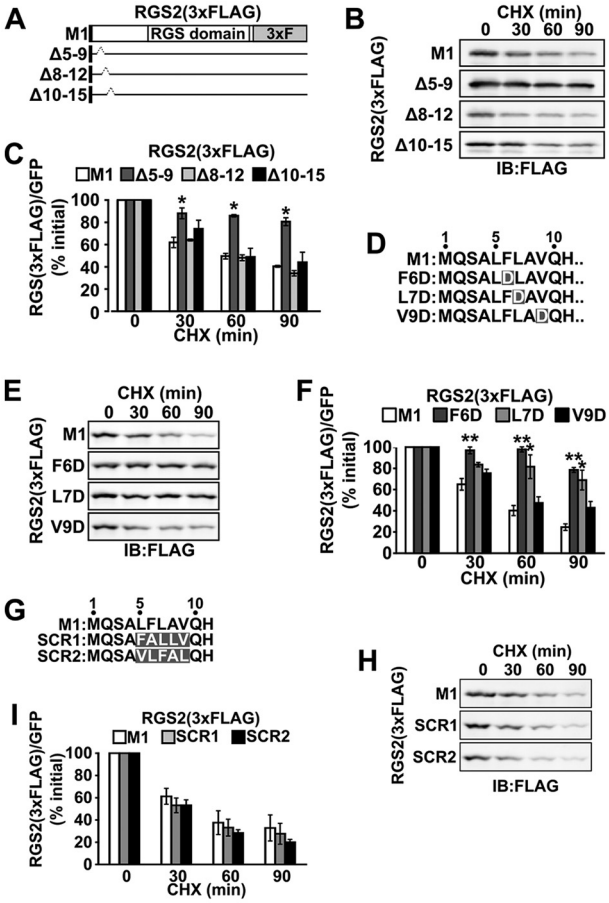

Figure 2. A novel hydrophobic degradation signal is located near the N terminus of RGS2. *A*, schematic of internal deletion mutants of Met-1–RGS2(3xFLAG). Mutants are designated by which residues were deleted as indicated by *dotted lines*. *B*, proteolytic degradation of deletion mutants following addition of CHX. *C*, quantification of degradation rates. *Error bars* denote S.E. *, $p < 0.05$ *versus* Met-1–RGS2(3xFLAG). *D*, N-terminal amino acid sequences of wild-type Met-1–RGS2(3xFLAG) and point mutant forms indicated by residues *highlighted*. *E*, proteolytic degradation of Met-1–RGS2(3xFLAG) and the indicated mutants following addition of CHX. *F*, quantification of RGS2(3xFLAG) protein levels detected by immunoblotting following addition of CHX. *Error bars* denote S.E. *, $p < 0.05$; **, $p < 0.01$ *versus* Met-1–RGS2(3xFLAG). *G*, N-terminal amino acid sequences of wild-type Met-1–RGS2(3xFLAG) and mutants (denoted SCR1 and SCR2) in which residues at positions 5–9 were scrambled as indicated by *highlighting*. *H*, proteolytic degradation of Met-1–RGS2(3xFLAG) and the indicated mutants following addition of CHX. *I*, quantification of RGS2(3xFLAG) protein levels detected by immunoblotting following addition of CHX. *Error bars* denote S.E. Data shown are representative of three or more independent experiments.

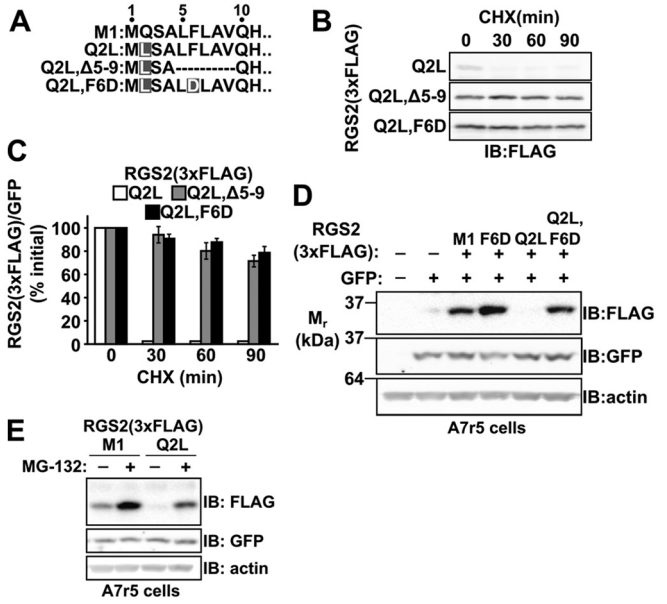

Figure 3. Proteolytic degradation of a hypertension-associated RGS2 missense mutant requires the N-terminal hydrophobic degradation signal. *A*, N-terminal amino acid sequences of wild-type Met-1–RGS2(3xFLAG), the hypertension-associated Q2L variant, and the Q2L variant bearing the indicated deletion and point mutations that inactivate the N-terminal hydrophobic degradation motif. *B*, proteolytic degradation of the indicated RGS2(3xFLAG) mutants following addition of CHX. *Error bars* denote S.E. *C*, quantification of degradation rates of the indicated RGS2(3xFLAG) mutants. *D*, relative expression levels of Met-1–RGS2(3xFLAG) and its indicated variants in A7r5 vascular smooth muscle cells. GFP and actin provided transfection and loading controls, respectively. *E*, proteasome-dependent expression of Met-1–RGS2(3xFLAG) and Met-1–RGS2-Q2L (3xFLAG) in A7r5 cells. Data shown are representative of three or more independent experiments.

or 10–15 had insignificant effect (Fig. 2, *B* and *C*), suggesting that the former deletion disrupted an internal degradation-promoting motif. This result also suggested that the N-terminal residue of RGS2 is not the sole determinant of proteolysis because the Δ5–9 mutant still contains a glutamine residue at position 2, which is hypothesized to promote degradation by the Ac/N-end rule.

Features of the degradation-promoting motif in residues 5–9 were identified by point mutagenesis of Met-1–RGS2 (3xFLAG). Because this region lacks charged or polar residues, its hydrophobic character may be functionally important. Indeed, substituting residues 6 or 7 with aspartic acid (Fig. 2*D*) markedly impaired degradation of Met-1–RGS2(3xFLAG) (Fig. 2, *E* and *F*), whereas an aspartic acid substitution at position 9 had insignificant effect (Fig. 2, *E* and *F*). In contrast, the specific amino acid sequence of this hydrophobic region was unimportant because scrambling its sequence (Fig. 2*G*) did not affect degradation kinetics (Fig. 2, *H* and *I*). Therefore, degradation of RGS2 requires a motif composed of hydrophobic residues near the N terminus.

Whereas the preceding results indicated that proteolytic degradation of wild-type RGS2 is not determined solely by the amino acid at position 2 according to the Ac/N-end rule, degradation of the hypertension-associated missense mutant (RGS2-Q2L) (5, 6, 46) nevertheless may be determined mainly by this mechanism because of the presence of a destabilizing leucine residue at position 2. We tested this hypothesis by determining the rate that Met-1–RGS2–Q2L(3xFLAG) is degraded in HEK 293 cells when residues 5–9 were deleted or the hydrophobic character of this region was disrupted by an F6D substitution (Fig. 3*A*). Results showed that the degradation of Met-1–RGS2–Q2L(3xFLAG) is strikingly impaired by either the Δ5–9 or F6D mutation (Fig. 3, *B* and *C*), indicating that the proteolytic degradation of this hypertension-associated form of RGS2 also requires this internal hydrophobic motif.

To determine whether this hydrophobic motif promotes degradation in vascular smooth muscle cells, in which RGS2 regulates vascular reactivity to control blood pressure (18, 41, 47), we analyzed expression of RGS2 as an indicator of protein stability in transfected A7r5 vascular smooth muscle cells (Fig. 3*D*). Consistent with prior studies of the hypertension-associ-

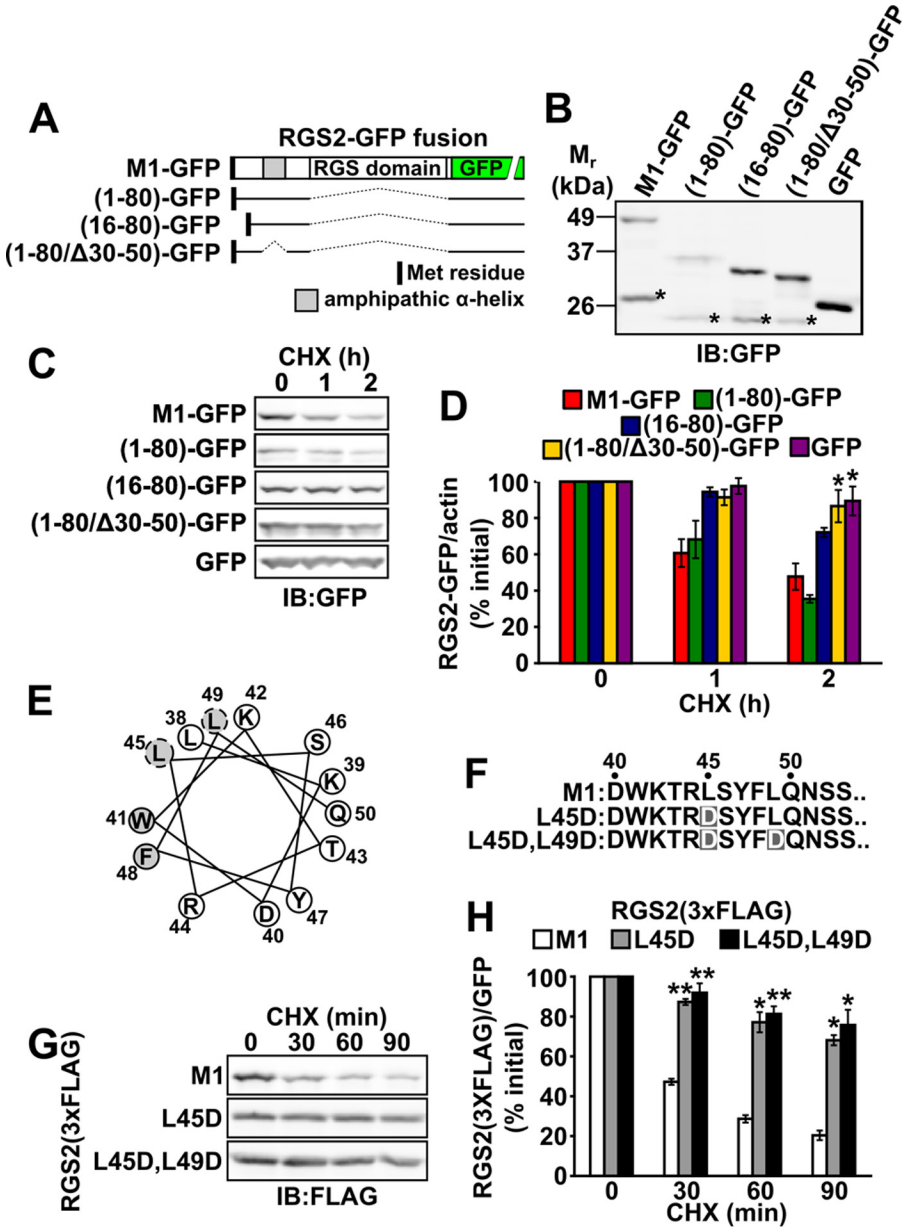

Figure 4. Proteolytic degradation of RGS2 requires an amphipathic α-helix. *A*, Met-1–RGS2-GFP fusion proteins. Met-1–GFP consists of full-length Met-1–RGS2 fused at its C terminus to GFP. The previously described amphipathic α-helix is indicated (*shaded*). Other fusion proteins are designated according to which portion of the RGS2 N-terminal domain was fused to GFP, or which portion within this domain was deleted, as indicated by residues within parentheses. *B*, expression of the indicated RGS2-GFP variants in transfected HEK 293 cells detected by immunoblotting. Proteolytically stable degradation products are indicated with *. *C*, proteolytic degradation of the indicated fusion proteins following addition of CHX. *D*, quantification of proteolytic degradation of the indicated fusion proteins. *Error bars* denote S.E. *, $p < 0.05$ *versus* (1–80)-GFP. *E*, helical wheel representation of the amphipathic α-helix, indicating the hydrophobic residues (*gray*) and mutated residues (*dashed circles*). *F*, amino acid sequence within the amphipathic α-helix and substitutions affecting its hydrophobic face (*highlighted* residues). *G*, proteolytic degradation of Met-1–RGS2(3xFLAG) and the indicated mutants following addition of CHX. *H*, quantification of RGS2(3xFLAG) protein levels detected by immunoblotting following addition of CHX. *Error bars* denote S.E. *, $p < 0.01$; **, $p < 0.001$ *versus* Met-1–RGS2(3xFLAG). Data shown are representative of three or more independent experiments.

ated RGS2(Q2L) mutant, the Q2L mutant form of Met-1–RGS2(3xFLAG) was poorly expressed in A7r5 cells (Fig. 3*D*) because of proteasome-mediated degradation (Fig. 3*E*). However, introducing the F6D substitution into Met-1–RGS2–Q2L(3xFLAG) dramatically increased expression in the absence of the proteasome inhibitor MG-132 (Fig. 3*D*). Similarly, controls showed that Met-1–RGS2–F6D(3xFLAG) was expressed more highly than wild-type Met-1–RGS2(3xFLAG). Thus, the hydrophobic motif proximal to the N terminus functions in a non-cell type–specific manner to determine the expression level of wild-type and a hypertension-associated mutant form of RGS2.

Although the preceding results indicated that a hydrophobic motif near the N terminus is required for RGS2 degradation, the results of further experiments indicated that this motif is insufficient to promote proteolysis and instead cooperates with a second internal signal composed of an amphipathic α-helix. This hypothesis was suggested initially by analyzing degradation of GFP fusion proteins bearing various regions of the RGS2 N-terminal domain (Fig. 4*A*). Fusing the entire N-terminal

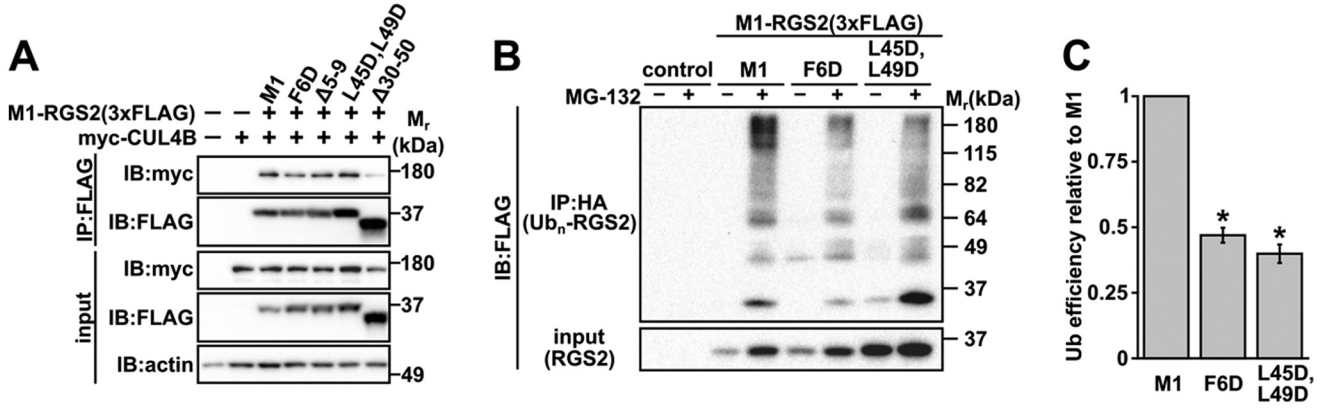

Figure 5. Proteolysis-resistant RGS2 mutants interact with CUL4B and reduce but do not eliminate ubiquitination. *A*, wild-type and proteolysis-resistant mutant forms of Met-1–RGS2(3xFLAG) interact with CUL4B. HEK 293 cells co-transfected with Myc-CUL4B and the indicated forms of RGS2(3xFLAG) were incubated with MG-132 for 4 h, lysed, immunoprecipitated with anti-FLAG (M2) affinity beads and analyzed by immunoblotting. *B*, ubiquitination of wild-type and proteolytically stable variants of Met-1–RGS2(3xFLAG). HEK 293 cells were co-transfected with HA-ubiquitin and the indicated variants of RGS2(3xFLAG), incubated with MG-132 for 8 h and immunoprecipitated with anti-HA agarose beads. Cell lysates and immunoprecipitates were analyzed by immunoblotting with anti-FLAG antibody to detect unmodified and ubiquitinated RGS2(3xFLAG) (designated Ub$_n$-RGS2). *C*, quantification of ubiquitination efficiency. The ratio of ubiquitinated RGS2 (IP:HA, IB:FLAG) to unubiquitinated RGS2 (input) (Ub$_n$-RGS2/RGS2) was quantified for the indicated forms of RGS2(3xFLAG) and normalized relative to the ubiquitination efficiency of Met-1–RGS2(3xFLAG). Statistical significance was determined by one way analysis of variance followed by Bonferroni post hoc test. *Error bars* denote S.E. *, $p < 0.001$ *versus* Met-1–RGS2(3xFLAG).

domain of RGS2 (residues 1–80) to GFP was sufficient to promote degradation relative to untagged GFP (Fig. 4, *B–D*). In contrast, deleting residues 30–50 of this RGS2-GFP fusion protein, which removes a previously described amphipathic α-helical region but preserves the N-terminal hydrophobic motif, strikingly impaired proteolytic degradation (Fig. 4, *B–D*), indicating that the hydrophobic N-terminal motif is insufficient. These results were extended by analyzing point mutations affecting the hydrophobic face of the amphipathic α-helical region of Met-1–RGS2(3xFLAG) (Fig. 4, *E–H*). Results showed that degradation of the L45D or L45D,L49D mutant forms of Met-1–RGS2(3xFLAG) was markedly impaired (Fig. 4, *G* and *H*). However, the amphipathic α-helical domain proved insufficient to promote degradation because a GFP fusion protein bearing residues 16–80 of RGS2, which removes the N-terminal hydrophobic motif but preserves the amphipathic α-helical motif (Fig. 4*A*), was as proteolytically stable as GFP (Fig. 4, *C* and *D*). Thus, apart from the identity of the amino acid residue at position 2, RGS2 degradation requires a novel bipartite degradation motif consisting of a hydrophobic region near the N terminus and an amphipathic α-helix located more distally.

The bipartite degradation signal of RGS2 is not essential for interaction with CUL4B or ubiquitination

To determine how this bipartite motif promotes proteolytic degradation of RGS2, we determined whether it is required for interaction with ubiquitin E3 ligases implicated previously in RGS2 degradation (36, 37). Interaction between Met-1–RGS2(3xFLAG) and a His-Myc–tagged form of the E3 ligase TEB4 was studied, but we were unable to detect interaction using previously reported chemical cross-linking and co-immunoprecipitation methods (see "Discussion").[3] In contrast, interaction between transiently expressed Met-1–RGS2 (3xFLAG) and E3 ubiquitin ligase complexes containing Myc-tagged CUL4B was detected readily by co-immunoprecipitation (Fig. 5*A*). However, this interaction was largely unaffected by mutations that dramatically impair RGS2 degradation (Fig. 5*A*), suggesting that these mutations blunt RGS2 proteolysis by events subsequent to E3 ligase interaction such as ubiquitin attachment or proteasome recognition. We therefore determined whether mutations that strongly impair proteolysis of RGS2 have concomitant effects on ubiquitination. Results showed that mutations disrupting either half of the bipartite degradation signal reduced but did not eliminate ubiquitination of transiently expressed Met-1–RGS2(3xFLAG) (Fig. 5, *B* and *C*). The bipartite degradation motif of RGS2 therefore affects ubiquitin conjugation.

RGS2 degradation determines agonist efficacy in $G_{q/11}$-coupled receptor signaling

Using our collection of RGS2 variants that are proteolyzed at different rates, we developed a system to determine how degradation impacts the ability of RGS2 to regulate $G_{q/11}$-coupled GPCR signaling. In contrast to assays used previously (ERK activity (37); inositol phosphate accumulation (35)) providing static measures of signaling end points, we used Ca^{2+} signaling to provide quantitative, kinetically resolved data to determine how RGS2 degradation impacts the amplitude or dynamics of agonist-evoked G_q signaling. For these purposes we used transfected Twitch-2B (48), a FRET reporter of Ca^{2+} signaling, to monitor agonist (carbachol) stimulation of $G_{q/11}$-coupled muscarinic receptors in HEK 293 cells transfected with wild-type or mutant forms of RGS2 that are degraded at different rates. We chose not to study mutants affecting the amphipathic α-helical region because they abrogate plasma membrane targeting and function of RGS2 (49); instead we studied mutations affecting the hydrophobic motif near the N terminus.

First, we determined whether proteolysis sets the expression level of RGS2 and affects the ability of this protein to regulate $G_{q/11}$-coupled GPCR-evoked Ca^{2+} signaling. Results showed that expression levels of the proteolytically stable F6D derivative and the proteolytically unstable Q2L derivative were, respectively, higher and lower than wild-

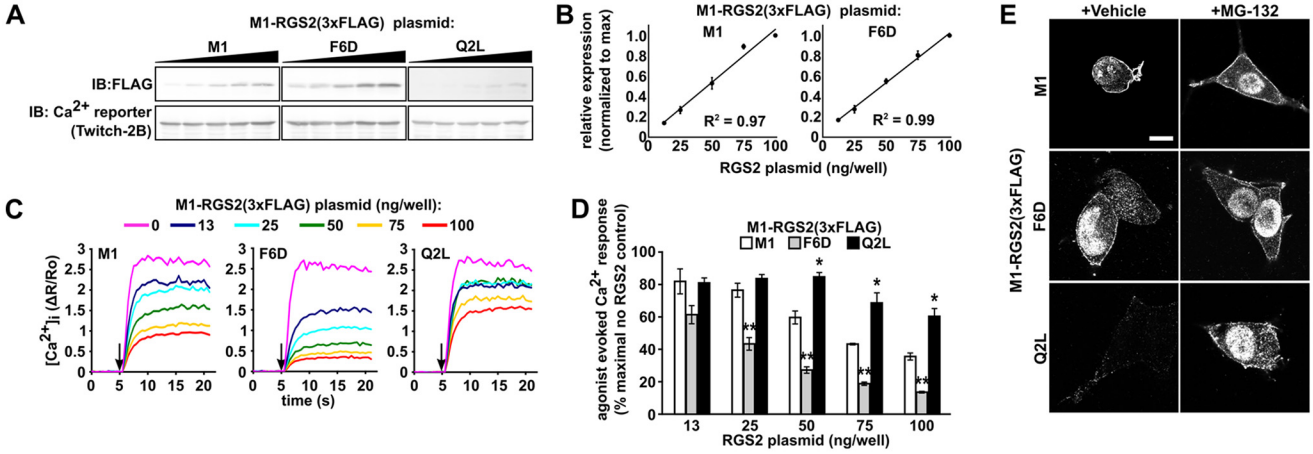

Figure 6. RGS2 degradation determines expression levels and agonist efficacy. *A*, proteolytic degradation sets protein expression levels of Met-1–RGS2(3xFLAG) and its variants. HEK 293 cells were co-transfected with a fixed amount of a plasmid expressing the Ca^{2+} FRET reporter Twitch-2B and increasing amounts of plasmid (13, 25, 50, 75, or 100 ng/well) expressing Met-1–RGS2(3xFLAG) or its Q2L and F6D variants. A single representative immunoblot is shown to indicate the relative expression of Met-1–RGS2(3xFLAG) and its variants with increasing amount of transfected plasmid DNA. Equal transfection efficiency was indicated by expression of Twitch-2B detected with a GFP antibody. *B*, expression of Met-1–RGS2(3xFLAG) and its F6D variant is linearly proportional to the amount of plasmid transfected; expression of the Q2L derivative was below the linear range, which precluded quantification. Quantified Met-1–RGS2(3xFLAG)/Twitch-2B ratios were plotted relative to the highest value observed. Correlation coefficients (R^2) of data fitted to a simple linear regression are indicated. *Error bars* indicate S.E. *C*, effect of increasing expression of Met-1–RGS2(3xFLAG) or its variants on $G_{q/11}$-coupled muscarinic receptor signaling. HEK 293 cells transfected as in (*A*) were treated at the indicated time (*arrow*) with carbachol (100 μM). Changes in $[Ca^{2+}]_i$ detected over time by the FRET reporter Twitch-2B are reported as ΔR/Ro. Experimental traces from cells transfected with various amounts of plasmid expressing Met-1–RGS2(3xFLAG) or its variants are color coded as indicated. Traces shown are averages of three independent experiments performed in triplicate. *D*, agonist efficacy as a function of Met-1–RGS2(3xFLAG) expression level. Agonist efficacy was quantified by normalizing peak Ca^{2+} response ((max ΔR/Ro with RGS2)/(max ΔR/Ro no RGS2) × 100). *Error bars* denote S.E. *, $p < 0.05$, **, $p < 0.001$ *versus* Met-1–RGS2(3xFLAG). *E*, subcellular localization of Met-1–RGS2(3xFLAG) and its variants in HEK 293 cells treated with vehicle or MG-132 as detected by fluorescence confocal microscopy. *Scale bar* is 10 μm. Data shown are representative of three or more independent experiments.

type Met-1–RGS2(3xFLAG) (Fig. 6*A*). Furthermore, expression of Met-1–RGS2(3xFLAG) and its F6D derivative were linearly proportional to the amount of transfected plasmid (Fig. 6, *A* and *B*). Expression of the Q2L derivative also increased with the amount of transfected plasmid (Fig. 6*A*), but below the linear range of detection. We then compared carbachol-evoked Ca^{2+} responses in HEK 293 cells lacking or expressing increasing levels of transfected wild-type or mutant forms of Met-1–RGS2(3xFLAG). In these cells, $G_{q/11}$ rather than $G_{i/o}$ mediates carbachol-evoked Ca^{2+} fluxes, as indicated by insensitivity to pertussis toxin.[3] A maximally effective concentration of carbachol evoked a rapid and robust Ca^{2+} response in control cells not transfected with RGS2 (Fig. 6*C*). In response to increasing levels of transfected wild-type MET-1–RGS2(3xFLAG), agonist efficacy (maximal Ca^{2+} response) diminished (Fig. 6, *C* and *D*). Expression of the proteolytically unstable Q2L mutant also reduced agonist efficacy, but required ~2-fold more transfected plasmid to produce an inhibitory effect equivalent to Met-1–RGS2(3xFLAG) (Fig. 6, *C* and *D*). Conversely, the slowly degraded F6D derivative required ~3-fold less transfected plasmid to elicit an effect equivalent to Met-1–RGS2(3xFLAG) (Fig. 6, *C* and *D*). These results were not because of differences in plasma membrane localization of Met-1–RGS2(3xFLAG) and its Q2L and F6D variants as indicated by fluorescence confocal microscopy (Fig. 6*E*), in contrast to the cytoplasmic mislocalization of RGS2 mutants bearing a disrupted amphipathic α-helix (49). Taken together these results indicated that proteolytic degradation regulates agonist efficacy in $G_{q/11}$-coupled GPCR signaling by determining expression levels of RGS2.

RGS2 degradation facilitates recovery of $G_{q/11}$-coupled GPCR signaling

RGS2 mRNA expression in many cell types is up-regulated strikingly and transiently in response to various GPCR agonists or other extracellular signals or second messengers, and then declines to baseline within ~1–2 h (29–31, 33), suggesting that this process potentially functions as a transiently acting feedback loop that blunts, or desensitizes, GPCR signaling. If so, proteolytic degradation could be important for determining not only peak RGS2 protein expression levels and the consequent magnitude of signal attenuation, as indicated above, but also the kinetics with which cells regain agonist responsiveness or resensitize as RGS2 mRNA expression declines, thereby terminating the inhibitory feedback loop.

We tested this hypothesis by adapting the Ca^{2+} signaling system described above to study how cells regain agonist responsiveness over time after synthesis of Met-1–RGS2 (3xFLAG) is stopped by blocking new protein synthesis with CHX. The proteasome dependence of the resensitization process was studied by performing experiments with or without the proteasome inhibitor MG-132, and by comparing cells transfected with wild-type, fast (Q2L), or slowly degrading (F6D) forms of Met-1–RGS2(3xFLAG). In each experiment transfected HEK 293 cells were treated with CHX with or without MG-132. At various times thereafter, cells were stimulated with a maximally effective concentration of carbachol. The recovery of agonist efficacy over time after RGS2 synthesis stops and proteolysis proceeds was determined by measuring peak agonist-evoked Ca^{2+} response following addition of CHX without or with MG-132. Control experiments using cells

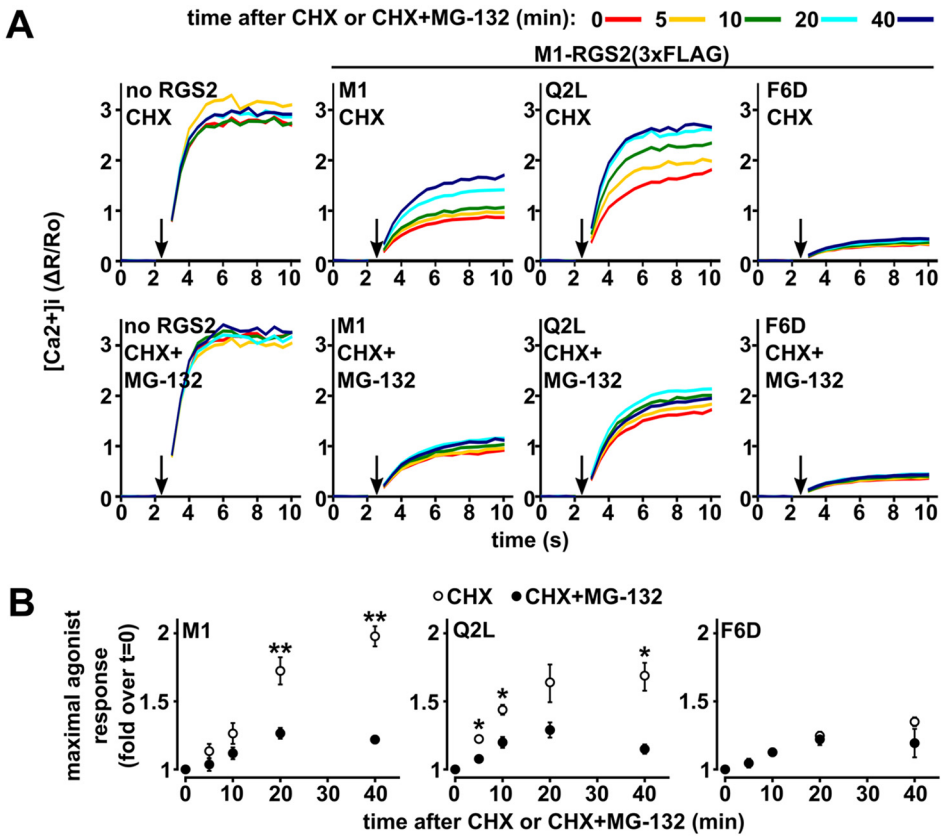

Figure 7. Proteasome-mediated degradation of RGS2 controls recovery of agonist responsiveness. *A*, recovery of agonist-evoked Ca^{2+} response (resensitization) depends on proteasome-mediated degradation of RGS2. HEK 293 cells co-transfected with Twitch-2B and pcDNA3.1 (no RGS2), Met-1–RGS2(3xFLAG) or its indicated variants were incubated with CHX without or with MG-132 for the indicated times (*color coded*) prior to stimulation with a maximally effective concentration of carbachol (*arrows*). Traces shown are averages of three independent experiments performed in triplicate. *B*, quantification of recovery of agonist responsiveness. Recovery was calculated as the -fold-increase in peak calcium response over time following addition of CHX without or with MG-132. *Error bars* indicate S.E. *, $p < 0.05$; **, $p < 0.01$ *versus* treatment with CHX + MG-132.

untransfected with RGS2 indicated that agonist efficacy changed insignificantly over 40 min after CHX treatment either without or with MG-132 (Fig. 7*A*), showing that during this time course the functions of endogenously expressed signaling or regulatory proteins are independent of proteasome-mediated degradation.

In contrast, clear evidence of proteasome-dependent resensitization was obtained with cells expressing wild-type Met-1–RGS2(3xFLAG). These cells initially exhibited blunted agonist response, which recovered significantly within 40 min after new protein synthesis was inhibited with CHX (Fig. 7, *A* and *B*). This recovery process was proteasome-dependent because it was blunted when cells were treated with CHX and MG-132 (Fig. 7, *A* and *B*). Similarly, cells expressing the unstable RGS2-Q2L(3xFLAG) mutant recovered agonist responsiveness in a proteasome-dependent manner (Fig. 7, *A* and *B*). However, in this case, recovery occurred more quickly, as expected if RGS2-Q2L(3xFLAG) is proteolyzed faster than Met-1–RGS2(3xFLAG). Conversely, cells expressing the slowly degrading RGS2-F6D(3xFLAG) mutant resensitized little within 40 min after CHX treatment either without or with MG-132 (Fig. 7, *A* and *B*). These results provided the first direct evidence indicating that proteasome-mediated degradation of RGS2 determines the rate and extent that cells recover agonist responsiveness once RGS2 expression ceases. Taken together, our findings indicate that proteolytic degradation of RGS2 can serve at least two functions: 1) determine agonist efficacy by setting expression levels of RGS2 protein and 2) determine the rate that cells recover agonist responsiveness as RGS2 expression declines.

RGS2 proteolysis regulates agonist-evoked contraction of resistance arteries

To explore the physiological significance of RGS2 proteolysis, we studied contraction of resistance arteries, which is regulated by RGS2 and critical for blood pressure control. Indeed, the absence of RGS2 augments vascular contraction evoked by $G_{q/11}$-coupled GPCR agonists (16, 47), and RGS2 mRNA expression in vascular smooth muscle cells is up- and then down-regulated following stimulation by angiotensin II (29). Accordingly, proteolytic degradation of RGS2 might facilitate recovery of vascular contractility as RGS2 mRNA expression declines.

To probe such regulatory processes in isolated resistance arteries, we explored whether vascular contractility is affected by proteolytic degradation of RGS2. Because the proteasome inhibitor MG-132 had complex effects on contraction of isolated mesenteric resistance arteries (MAs), we instead determined whether blocking protein synthesis with CHX affects vascular contraction. We reasoned that if endogenous RGS2 is

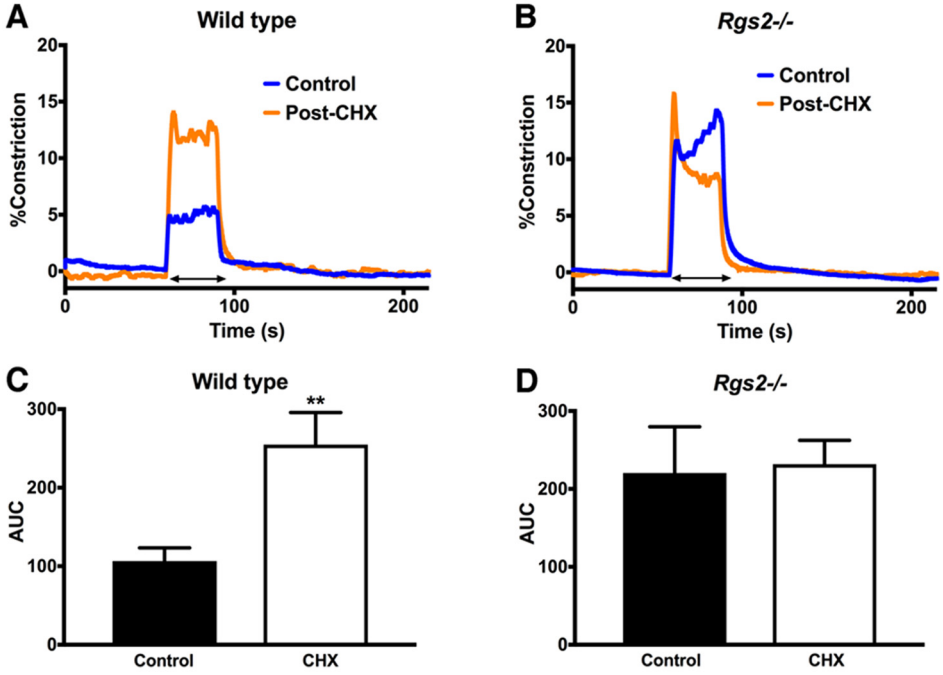

Figure 8. Proteolytic degradation of RGS2 regulates $G_{q/11}$-evoked constriction of resistance arteries. *A* and *B*, representative traces showing constriction of vehicle control (*blue*) or CHX-treated (1 h) (*orange*) wild-type (*A*) or RGS2-deficient (*B*) mesenteric arteries in response to 30 s electrical field stimulation (*bidirectional arrows*). Traces representative of six independent experiments performed with one vessel per animal for each genotype indicate the percentage change in lumen diameter (% constriction) relative to baseline. *C* and *D*, quantitation of EFS-induced vasoconstriction. The magnitude of EFS-induced constriction was calculated as the area under the curve (AUC). Mean AUC values ± S.E. are shown. **, $p < 0.01$ *versus* control.

proteolytically unstable in wild-type MAs, CHX treatment should phenocopy genetic deletion of RGS2.

We tested this prediction by using submaximal electrical field stimulation (EFS) (40 V at 15 Hz) of MAs to release endogenous norepinephrine and ATP from sympathetic nerve terminals embedded in the vessel wall, thereby activating $G_{q/11}$-coupled α_1-adrenergic and P2Y2 purinergic GPCRs in vascular smooth muscle cells and triggering vasoconstriction (51–53). If the proteolytic half-life of RGS2 in MAs is similar to that of transfected RGS2 (~30 min), then treating wild-type MAs 1 h with CHX would be sufficient for most of the preexisting pool of RGS2 to be degraded. Indeed, we found that treating wild-type MAs 1 h with CHX augmented EFS-evoked contraction 2.5-fold relative to vehicle controls (Fig. 8, *A* and *B*). As expected if this effect was caused by degradation of RGS2, it phenocopied the magnitude of EFS-evoked contraction in vehicle-treated *Rgs2*$^{-/-}$ MAs (Fig. 8, *C* and *D*). Moreover, CHX failed to augment contraction of *Rgs2*$^{-/-}$ MAs (Fig. 8, *C* and *D*), indicating that other signaling or contractile proteins were affected insignificantly by CHX treatment. Accordingly, these results support the hypothesis that proteolytic degradation of RGS2 in resistance arteries occurs at rates competent to control agonist responsiveness on physiologically relevant time scales.

Discussion

Here we have shown that proteolytic degradation of RGS2 facilitates temporal regulation of $G_{q/11}$-mediated signaling and vascular contraction. We also have shown that mechanisms mediating proteolytic degradation of RGS2 are considerably more complex than appreciated previously.

In several cell types and organs, RGS2 mRNA expression is strikingly and transiently up- and then down-regulated in response to various extracellular stimuli, GPCR agonists, or second messengers, potentially providing negative feedback of signaling pathways controlled by RGS2 (34). By affecting the level of RGS2 protein expressed, proteolytic degradation is capable of determining the magnitude of the inhibitory effect achieved by up-regulating RGS2 mRNA expression. Moreover, because our results show that proteolysis of RGS2 is kinetically competent to determine how quickly agonist responsiveness recovers after RGS2 expression ceases, this process also is capable of determining the rate that feedback regulation of cell signaling is relieved as RGS2 mRNA expression declines. Additional mechanisms are likely to influence such outcomes because cardiotonic steroids, PKC, and cGK can regulate RGS2 proteolysis (38–41), providing further control of feedback regulation of GPCR signaling by RGS2.

Our findings indicate that RGS2 proteolysis is more complex mechanistically than appreciated previously. Beyond prior understanding that RGS2 proteolysis via the Ac/N-end rule pathway depends on N-terminal acetylation and the identity of the amino acid at position 2 of the longest alternative translation product (37), we have found that RGS2 degradation requires a novel bipartite signal consisting of a hydrophobic region proximal to the N terminus and an amphipathic α-helical region located more distally.

This novel bipartite degradation signal of RGS2 may facilitate proteolysis by several mechanisms. First, this signal may be recognized directly by TEB4 (MARCH6) in the Ac/N-end rule pathway. Indeed, TEB4 can bind *in vitro* to the first 10 residues of RGS2 (37), which includes the N-terminal hydrophobic region of the bipartite degradation motif but excludes the amphipathic α-helix. However, determining whether TEB4-

RGS2 binding mediates RGS2 degradation was precluded by our failure to detect this interaction in cells despite using previously reported chemical cross-linking methods (37). Second, TEB4 might recognize the amphipathic α-helix of RGS2 because degradation signals in substrates targeted by the yeast TEB4 homolog Doa10 include exposed hydrophobic faces of amphipathic α-helices (54). Third, the bipartite degradation motif of RGS2 might be recognized indirectly by TEB4, as suggested by studies of Doa10 showing that some substrates are presented indirectly by Hsp70 and Hsp40 chaperones and co-chaperones (55). Fourth, the bipartite degradation signal of RGS2 may be recognized indirectly by the CUL4B/DDB1/FBXO44 E3 ligase complex that target RGS2 for degradation, because neither half of this signal is required for physical interaction between RGS2 and CUL4-containing complexes.

The bipartite degradation signal of RGS2 may function in other steps of the proteolysis process. Indeed, our finding that mutations disrupting these signals reduce but do not eliminate ubiquitination of RGS2 is consistent with evidence in other systems that degradation signals can affect selection of lysine acceptor sites for ubiquitination, the efficiency of ubiquitin transfer to substrates, or recognition or unfolding of ubiquitinated substrates by the proteasome (56–59).

Mechanisms regulating the proteolysis of RGS2 also remain to be elucidated in detail. Cardiotonic steroids, PKC, or cGK all regulate RGS2 degradation (38–41), although whether these mechanisms directly target RGS2 or the machinery that mediates RGS2 degradation is unclear. PKC can directly phosphorylate RGS2, but whether this is sufficient to inhibit RGS2 degradation has not been determined. Regulation of RGS2 degradation by cGK activity apparently occurs by more than one mechanism because inhibition of this protein kinase blunts RGS2 degradation whereas inactivation of the cGK phosphorylation sites in RGS2 promotes proteolysis.

In conclusion, by showing that proteolytic degradation of RGS2 can facilitate temporal regulation of agonist responsiveness on physiologically relevant time scales, our findings suggest that targeting proteolytic mechanisms might provide avenues for treating diseases such as hypertension and anxiety that have been linked to decreased RGS2 expression or function. Various steps in processes that control proteolytic degradation of RGS2 therefore may provide a multiplicity of targets to pursue for therapy.

Experimental procedures

cDNAs

The plasmid pcDNA3.1 (Thermo Fisher Scientific) was used to drive expression of all RGS2 constructs used in this study. All constructs were prepared by PCR cloning using KAPA Taq polymerase (Kapa Biosystems, catalog no. KK1006). All point mutations were generated by site-directed mutagenesis, and all deletion mutants were made by PCR-mediated ligation. Met-1–RGS2(3xFLAG) used as a template for all RGS2 expression constructs was generated by mutating all internal translation start sites (ATG) to leucine (CTG). GFP fusion proteins were generated by cloning PCR amplified fragments of RGS2 into plasmid pcDNA3.1-N-MCS-GFP, which was generated by cloning GFP from eGFP-N (Clontech) into pcDNA3.1. Twitch-2B pcDNA3, which expresses a FRET-based Ca^{2+} reporter, was a gift of Oliver Griesbeck (Addgene plasmid, catalog no. 49531) (48). Expression plasmids for Myc-CUL4B and HA-ubiquitin were gifts from Helen Piwnica-Worms (University of Texas MD Anderson Cancer Center). A plasmid expressing TEB4-His-Myc was a gift of Mark Hochstrasser (Yale University School of Medicine).

Antibodies and reagents

Mouse anti-FLAG (M2) (Sigma, catalog no. F1804); mouse anti-actin (C4) (Millipore, catalog no. MAB1501); rabbit anti-GFP (Abcam, catalog no. ab290, various lots); Odyssey infrared secondary antibodies: goat anti-mouse IRDye 800CW (LI-COR, catalog no. 926–32210, lot C30702–01), goat anti-rabbit IRDye 680RD (LI-COR, catalog no. 926–68071, lot C3081502), HRP conjugated mouse anti-FLAG (M2) (Sigma, catalog no. A8592), HRP conjugated mouse anti-MYC (9e10) (Thermo Fisher Scientific, catalog no. MA1–980-HRP, lot RD232005), mouse anti-FLAG (M2) affinity gel (Sigma, catalog no. A2220, various lots), mouse anti-HA agarose (Sigma, catalog no. A2095, lot 026M4810V), cycloheximide (Sigma, catalog no. C7698), MG-132 (Calbiochem, catalog no. 47479D), carbamoylcholine chloride/carbachol (Sigma, catalog no. C4382).

Cell culture and transfection

HEK 293 and A7r5 cells (ATCC, CRL-1444) were grown in DMEM/F-12 (Thermo Fisher Scientific, catalog no. 11330–032) with 10% FBS (Atlanta Biologicals, catalog no. S11150) and penicillin/streptomycin (Thermo Fisher Scientific, catalog no. 15140122) at 37 °C and 5% CO_2 in a humidified incubator. Most transfections were performed with TransIT-LT1 (Mirus Bio, catalog no. MIR2305) according to the manufacturer's protocol.

Protein degradation assay

HEK 293 cells were co-transfected with the indicated RGS2(3xFLAG) variants and GFP or transfected with the indicated RGS2-GFP fusion variant for 20–24 h. Transfected cells were treated with cycloheximide (30 μg/ml) for the indicated times, lysed, and harvested in radioimmunoprecipitation assay (RIPA) buffer (150 mM sodium chloride, 1% Triton X-100, 0.5% sodium deoxycholate, 0.1% sodium dodecyl sulfate, 50 mM Tris, pH 8.0) with 1× cOmplete Protease Inhibitor (Roche, catalog no. 11697498001). Cleared lysates were mixed with Laemmli buffer (25% v/v glycerol, 2% w/v sodium dodecyl sulfate, 0.01% w/v bromophenol blue, 62.5 mM Tris pH 6.8) and processed for Western blot analysis with the Odyssey Infrared Imaging System (LI-COR).

Western blot detection with the Odyssey Infrared Imaging System

Lysates were resolved with 15% SDS-PAGE and transferred to Immobilon(P)-FL fluorescence optimized PVDF membrane (Millipore, catalog no. IPFL00010). Membranes were incubated in blocking buffer (5% w/v milk in TBST (25 mM Tris pH 7.2, NaCl 150 mM, 2.7 mM KCl, 0.1% v/v Tween 20)) and then with the appropriate primary antibody (mouse anti-FLAG (M2),

rabbit anti-GFP (ab290), or mouse anti-actin (C4)). Membranes were washed with TBST at least three times, incubated with the appropriate infrared dye-conjugated secondary antibody (anti-mouse IR800 or anti-rabbit IR680), washed at least three times, and imaged with Odyssey Infrared Scanner. Data were quantified with image analysis software Odyssey v2.1. For assays involving RGS2(3xFLAG) variants, Western blot signals for FLAG were normalized to GFP. For assays involving RGS2-GFP fusion variants, Western blot signals for GFP were normalized to actin. Relative protein levels are expressed as the percentage of RGS2(3xFLAG)/GFP or RGS2-GFP/actin at time = 0. A standard curve relating protein expression to signal intensity was generated to establish the linear range of detection. Only signals within the linear range of detection were quantified and used for analysis. At least three independent experiments were performed for each analysis.

Western blotting procedure for detection by chemiluminescence

Lysates were prepared and resolved with SDS-PAGE as described above, and transferred to Immobilon-P PVDF membrane (Millipore, catalog no. IPVH00010). Membranes were processed as above and incubated with appropriate primary and secondary antibodies. Membranes were incubated with Clarity Western ECL Substrate (Bio-Rad Laboratories, catalog no. 170–5060) and imaged with ChemiDoc Imaging System (Bio-Rad Laboratories).

Co-immunoprecipitation of RGS2 with CUL4

HEK 293 cells co-transfected with Myc-tagged CUL4B and the indicated RGS2(3xFLAG) variants were incubated with MG-132 (10 μM) for 4 h, lysed, and harvested in radioimmunoprecipitation assay buffer. Cleared lysates were immunoprecipitated with anti-FLAG (M2) affinity gel and eluted by boiling in Laemmli buffer. Lysates and eluates were resolved by 12% SDS-PAGE, transferred to PVDF, and processed for Western blotting. FLAG- and Myc-tagged proteins were detected with HRP-conjugated anti-FLAG (M2) and HRP-conjugated anti-Myc (9e10) primary antibodies, respectively.

Immunoprecipitation of proteins conjugated to HA-tagged ubiquitin

HEK 293 cells co-transfected with HA-tagged ubiquitin and the indicated RGS2(3xFLAG) variants were incubated with vehicle (DMSO) or MG-132 (10 μM) for 8 h and lysed in PBS/Triton X-100 buffer (1 mM potassium phosphate, 155 mM sodium chloride, 3 mM sodium phosphate, 1% v/v Triton X-100, 10 mM *N*-ethylmaleimide (Pierce, catalog no. 23030), 1× cOmplete Protease Inhibitor). Cleared lysates were immunoprecipitated with anti-HA agarose and eluted by boiling in Laemmli buffer. Lysates and eluates were resolved by 12% SDS-PAGE, transferred to PVDF, and processed for Western blotting as described above. FLAG-tagged RGS2 was detected with HRP-conjugated anti-FLAG (M2) primary antibody. Western blots were quantified with Image Lab (Bio-Rad Laboratories). A standard curve for protein amount to signal intensity was generated to establish the linear range of detection. Only signals within the linear range of detection were used.

Agonist-evoked Ca^{2+} flux assay

HEK 293 cells co-transfected with FRET-based Ca^{2+} sensor Twitch-2B (48) and the indicated RGS2(3xFLAG) variants were plated on a 96-well clear bottom black wall plate (Costar, catalog no. 3603) coated with poly-D-lysine (Sigma, catalog no. P0899). 20–24 h later, the culture medium was replaced with imaging buffer (125 mM NaCl, 5 mM KCl, 1.5 mM $MgCl_2$, 1.5 mM $CaCl_2$, 10 mM D-glucose, 20 mM HEPES, pH 7.4) (60) and assayed immediately at 37 °C with a Synergy H4 Hybrid Reader (BioTek) equipped with an injection pump. For assays in Fig. 7, cells were preincubated in CHX/MG-132 in imaging buffer for the indicated time periods prior to agonist stimulation. For all assays, baseline $[Ca^{2+}]_i$ was measured first, then cells were stimulated by agonist injection and measurement of $[Ca^{2+}]_i$ resumed until signals plateaued. FRET detected by Twitch-2B was measured every 49 ms by exciting the FRET donor with 420/20 bandpass filter, and simultaneously detecting donor and acceptor emissions with 480/20 and 540/20 bandpass filters, respectively. A dichroic mirror with a 455-nm cutoff was used to separate excitation and emission light paths. FRET, or changes in $[Ca^{2+}]_i$, was expressed ratiometrically, as seen in Equation 1:

$$\frac{\Delta R}{Ro} = \frac{\text{FRET ratio} - \text{baseline FRET ratio}}{\text{baseline FRET ratio}} \qquad \text{(Eq. 1)}$$

where FRET ratio = ($540\ nm^{emission}/480\ nm^{emission}$) at any time point, and the baseline FRET ratio = average of ($540\ nm^{emission}/480\ nm^{emission}$) prior to agonist stimulation.

Confocal microscopy

HEK 293 cells were transfected using Lipofectamine 2000 (Thermo Fisher Scientific, catalog no. 11668) according to the manufacturer's protocol. After 6 h, the cells were plated on poly-D-lysine (1 μg/ml) coated glass coverslips and incubated for 24 h. Cells were treated 4 h with MG-132 (10 μM) or vehicle (DMSO). Cells were fixed with 4% paraformaldehyde in PBS for 15 min at room temperature and washed with PBS. Fixed cells were permeabilized with 0.5% Triton X-100 in PBS for 10 min at room temperature. Cells then were incubated for at least 30 min at room temperature in blocking buffer (1% BSA (Sigma catalog no. A2153), 0.1% cold water fish skin gelatin (Sigma, catalog no. G7765), 0.3% Triton X-100 in PBS). Cells were incubated with mouse anti-FLAG (M2) primary antibody (Sigma, catalog no. F1804, lot. SLBN5629V) in blocking buffer overnight at 4 °C, followed by washes with PBS containing 0.3% Triton X-100. Cells were incubated in anti-mouse Alexa Fluor 488 secondary antibody (Invitrogen, catalog no. A11001, lot 1696425) in blocking buffer containing 5% goat serum (Sigma, catalog no. G9023) at room temperature for 1 h and then washed with 0.3% Triton X-100 PBS. The coverslips were mounted in VECTASHIELD Antifade Mounting Medium containing DAPI (Vector Laboratories, catalog no. H-1200).

Animals

All animal experiments were conducted under protocols approved by the Institutional Animal Care and Use Committee of Drexel University, in accordance with the U.S. Animal Wel-

fare Act. Experiments used congenic 2- to 3-month-old male and female *Rgs2*$^{-/-}$ and wild-type mice in the Charles River C57BL/6 genetic background. The generation of *Rgs2*$^{-/-}$ mice has been described previously (15). Mice were provided access to food and water *ad libitum* in facilities maintained at 22 °C with a 12-h light/dark cycle.

Mesenteric artery contraction studies

Mice were euthanized by deep anesthesia with ketamine/xylazine (ketamine, 43 mg/kg, i.p., and xylazine, 6 mg/kg, i.p.) followed by cervical dislocation. The gut was excised and placed in chilled physiological saline solution buffer with the following composition (mM): 140 NaCl, 5 KC1, 1.2 $MgSO_4$, 2.0 $CaC1_2$, 10 sodium acetate, 10 HEPES, 1.2 $Na_2H_2PO_4$, 5 glucose, and pH adjusted to 7.4 with NaOH. Second order mesenteric arteries and their associated nerve terminals were isolated and transferred into a vessel chamber, cannulated at both ends with glass pipettes, and secured with nylon ligature as described previously (50). Intraluminal pressure and vessel bath temperature were maintained by servo-controlled pressure pump and temperature control systems. The vessel lumen and chamber were filled with PSS buffer. After 30 min equilibration at 37 °C and 60 mmHg, vessel viability was tested with increasing concentrations (20, 40, 60, 80 mM) of high potassium-PSS solution to assess maximal intrinsic contraction. After extensive washing with PSS buffer, electrical field stimulation (40 V, at 15 Hz for 30 s) was used to release endogenous neurotransmitter (norepinephrine) and elicit receptor-evoked contraction. Cannulated vessels from wild-type and *Rgs2*$^{-/-}$ mice were subjected once to EFS-induced constriction, followed by 15 min washout with PSS buffer. Arteries then were incubated with CHX (30 μg/ml for 1h) to block synthesis of RGS2, allowing proteolytic degradation to occur before a second EFS stimulus was applied. EFS-induced vasoconstriction was recorded as the percentage of reduction from baseline of vessel lumen diameter, and quantified as the total area under the curve (AUC) during EFS (30 s). AUC data were calculated as mean values ± S.E.

Statistical analysis

Unless stated otherwise, statistical significance was determined with two-way analysis of variance (ANOVA) followed by Bonferroni post hoc test. Paired Student's *t* test was used for statistical analysis of artery contraction data.

Author contributions—S. M. K. conducted and analyzed most of the experiments. J. G. R. conducted experiments in Fig. 6*E*. A. J. E. and P. O.-O. conducted experiments in Fig. 8. K. J. B. and S. M. K. designed experiments and wrote the paper. K. J. B. conceived the project.

Acknowledgments—We thank members of the Blumer lab for comments on the manuscript, and Drs. Peirong Hu and Sharon Young for contributions during initial phases of this study. Confocal microscopy facilities in the Washington University Center for Cellular Imaging (WUCCI) were supported by Washington University School of Medicine, The Children's Discovery Institute of Washington University and St. Louis Children's Hospital (CDI-CORE-2015–505), and the National Institute for Neurological Disorders and Stroke (NS086741).

References

1. Gainetdinov, R. R., Premont, R. T., Bohn, L. M., Lefkowitz, R. J., and Caron, M. G. (2004) Desensitization of G protein–coupled receptors and neuronal functions. *Annu. Rev. Neurosci.* **27,** 107–144
2. Neubig, R. R. (2015) RGS-insensitive G proteins as *in vivo* probes of RGS function. *Prog. Mol. Biol. Transl. Sci.* **133,** 13–30
3. Kimple, A. J., Bosch, D. E., Giguère, P. M., and Siderovski, D. P. (2011) Regulators of G-protein signaling and their Gα substrates: Promises and challenges in their use as drug discovery targets. *Pharmacol. Rev.* **63,** 728–749
4. Nishiguchi, K. M., Sandberg, M. A., Kooijman, A. C., Martemyanov, K. A., Pott, J. W., Hagstrom, S. A., Arshavsky, V. Y., Berson, E. L., and Dryja, T. P. (2004) Defects in RGS9 or its anchor protein R9AP in patients with slow photoreceptor deactivation. *Nature* **427,** 75–78
5. Yang, J., Kamide, K., Kokubo, Y., Takiuchi, S., Tanaka, C., Banno, M., Miwa, Y., Yoshii, M., Horio, T., Okayama, A., Tomoike, H., Kawano, Y., and Miyata, T. (2005) Genetic variations of regulator of G-protein signaling 2 in hypertensive patients and in the general population. *J. Hypertens.* **23,** 1497–1505
6. Riddle, E. L., Rana, B. K., Murthy, K. K., Rao, F., Eskin, E., O'Connor, D. T., and Insel, P. A. (2006) Polymorphisms and haplotypes of the regulator of G protein signaling-2 gene in normotensives and hypertensives. *Hypertension* **47,** 415–420
7. Ross, E. M., and Wilkie, T. M. (2000) GTPase-activating proteins for heterotrimeric G proteins: Regulators of G protein signaling (RGS) and RGS-like proteins. *Annu. Rev. Biochem.* **69,** 795–827
8. Sethakorn, N., Yau, D. M., and Dulin, N. O. (2010) Non-canonical functions of RGS proteins. *Cell. Signal.* **22,** 1274–1281
9. Heximer, S. P., Watson, N., Linder, M. E., Blumer, K. J., and Hepler, J. R. (1997) RGS2/G0S8 is a selective inhibitor of Gqα function. *Proc. Natl. Acad. Sci. U.S.A.* **94,** 14389–14393
10. Heximer, S. P., Srinivasa, S. P., Bernstein, L. S., Bernard, J. L., Linder, M. E., Hepler, J. R., and Blumer, K. J. (1999) G protein selectivity is a determinant of RGS2 function. *J. Biol. Chem.* **274,** 34253–34259
11. Ingi, T., Krumins, A. M., Chidiac, P., Brothers, G. M., Chung, S., Snow, B. E., Barnes, C. A., Lanahan, A. A., Siderovski, D. P., Ross, E. M., Gilman, A. G., and Worley, P. F. (1998) Dynamic regulation of RGS2 suggests a novel mechanism in G-protein signaling and neuronal plasticity. *J. Neurosci.* **18,** 7178–7188
12. Kimple, A. J., Soundararajan, M., Hutsell, S. Q., Roos, A. K., Urban, D. J., Setola, V., Temple, B. R. S., Roth, B. L., Knapp, S., Willard, F. S., and Siderovski, D. P. (2009) Structural determinants of G-protein α subunit selectivity by regulator of G-protein signaling 2 (RGS2). *J. Biol. Chem.* **284,** 19402–19411
13. Sinnarajah, S., Dessauer, C. W., Srikumar, D., Chen, J., Yuen, J., Yilma, S., Dennis, J. C., Morrison, E. E., Vodyanoy, V., and Kehrl, J. H. (2001) RGS2 regulates signal transduction in olfactory neurons by attenuating activation of adenylyl cyclase III. *Nature* **409,** 1051–1055
14. Lutz, S., Freichel-Blomquist, A., Yang, Y., Rümenapp, U., Jakobs, K. H., Schmidt, M., and Wieland, T. (2005) The guanine nucleotide exchange factor p63RhoGEF, a specific link between $G_{q/11}$-coupled receptor signaling and RhoA. *J. Biol. Chem.* **280,** 11134–11139
15. Oliveira-dos-Santos, A. J., Matsumoto, G., Snow, B. E., Bai, D., Houston, F. P., Whishaw, I. Q., Mariathasan, S., Sasaki, T., Wakeham, A., Ohashi, P. S., Roder, J. C., Barnes, C. A., Siderovski, D. P., and Penninger, J. M. (2000) Regulation of T cell activation, anxiety, and male aggression by RGS2. *Proc. Natl. Acad. Sci. U.S.A.* **97,** 12272–12277
16. Heximer, S. P., Knutsen, R. H., Sun, X., Kaltenbronn, K. M., Rhee, M.-H., Peng, N., Oliveira-dos-Santos, A., Penninger, J. M., Muslin, A. J., Steinberg, T. H., Wyss, J. M., Mecham, R. P., and Blumer, K. J. (2003) Hypertension and prolonged vasoconstrictor signaling in RGS2-deficient mice. *J. Clin. Invest.* **111,** 445–452
17. Tang, K. M., Wang, G.-R., Lu, P., Karas, R. H., Aronovitz, M., Heximer, S. P., Kaltenbronn, K. M., Blumer, K. J., Siderovski, D. P., Zhu, Y., and Mendelsohn, M. E. (2003) Regulator of G-protein signaling-2 mediates vascular smooth muscle relaxation and blood pressure. *Nat. Med.* **9,** 1506–1512

18. Sun, X., Kaltenbronn, K.M., Steinberg, T.H., Blumer, K.J. (2005) RGS_2 is a mediator of nitric oxide action on blood pressure and vasoconstrictor signaling. *Mol. Pharmacol.* **67,** 631–639
19. Gurley, S. B., Griffiths, R. C., Mendelsohn, M. E., Karas, R. H., and Coffman, T. M. (2010) Renal actions of RGS2 control blood pressure. *J. Am. Soc. Nephrol.* **21,** 1847–1851
20. Osei-Owusu, P., Owens, E. A., Jie, L., Reis, J. S., Forrester, S. J., Kawai, T., Eguchi, S., Singh, H., and Blumer, K. J. (2015) Regulation of renal hemodynamics and function by RGS2. *PLoS One* **10,** e0132594
21. Zhang, W., Anger, T., Su, J., Hao, J., Xu, X., Zhu, M., Gach, A., Cui, L., Liao, R., Mende, U. (2006) Selective loss of fine tuning of $G_{q/11}$ signaling by RGS2 protein exacerbates cardiomyocyte hypertrophy. *J. Biol. Chem.* **281,** 5811–5820
22. Takimoto, E., Koitabashi, N., Hsu, S., Ketner, E. A., Zhang, M., Nagayama, T., Bedja, D., Gabrielson, K. L., Blanton, R., Siderovski, D. P., Mendelsohn, M. E., and Kass, D. A. (2009) Regulator of G protein signaling 2 mediates cardiac compensation to pressure overload and antihypertrophic effects of PDE5 inhibition in mice. *J. Clin. Invest.* **119,** 408–420
23. Park-Windhol, C., Zhang, P., Zhu, M., Su, J., Chaves, L., Jr., Maldonado, A. E., King, M. E., Rickey, L., Cullen, D., and Mende, U. (2012) Gq/11-mediated signaling and hypertrophy in mice with cardiac-specific transgenic expression of regulator of G-protein signaling 2. *PLoS One.* **7,** e40048
24. Yalcin, B., Willis-Owen S. A. G., Fullerton, J., Meesaq, A., Deacon, R. M., Rawlins, J. N. P., Copley, R. R., Morris, A. P., Flint, J., and Mott, R. (2004) Genetic dissection of a behavioral quantitative trait locus shows that *Rgs2* modulates anxiety in mice. *Nat. Genet.* **36,** 1197–1202
25. Hurst, J. H., and Hooks, S. B. (2009) Regulator of G-protein signaling (RGS) proteins in cancer biology. *Biochem. Pharmacol.* **78,** 1289–1297
26. Semplicini, A., Lenzini, L., Sartori, M., Papparella, I., Calò, L. A., Pagnin, E., Strapazzon, G., Benna, C., Costa, R., Avogaro, A., Ceolotto, G., and Pessina, A. C. (2006) Reduced expression of regulator of G-protein signaling 2 (RGS2) in hypertensive patients increases calcium mobilization and ERK1/2 phosphorylation induced by angiotensin II. *J. Hypertens.* **24,** 1115–1124
27. Siderovski, D. P., Heximer, S. P., and Forsdyke, D. R. (1994) A human gene encoding a putative basic helix–loop–helix phosphoprotein whose mRNA increases rapidly in cycloheximide-treated blood mononuclear cells. *DNA Cell Biol.* **13,** 125–147
28. Heximer, S. P., Cristillo, A. D., and Forsdyke, D. R. (1997) Comparison of mRNA expression of two regulators of G-protein signaling, RGS1/BL34/1R20 and RGS2/G0S8, in cultured human blood mononuclear cells. *DNA Cell Biol.* **16,** 589–598
29. Grant, S. L., Lassègue, B., Griendling, K. K., Ushio-Fukai, M., Lyons, P. R., and Alexander, R. W. (2000) Specific regulation of RGS2 messenger RNA by angiotensin II in cultured vascular smooth muscle cells. *Mol. Pharmacol.* **57,** 460–467
30. Ko, J. K., Choi, K. H., Kim, I. S., Jung, E. K., and Park, D. H. (2001) Inducible RGS2 is a cross-talk regulator for parathyroid hormone signaling in rat osteoblast-like UMR106 cells. *Biochem. Biophys. Res. Commun.* **287,** 1025–1033
31. Roy, A. A., Nunn, C., Ming, H., Zou, M.-X., Penninger, J., Kirshenbaum, L. A., Dixon, S. J., and Chidiac, P. (2006) Up-regulation of endogenous RGS2 mediates cross-desensitization between G_s and G_q signaling in osteoblasts. *J. Biol. Chem.* **281,** 32684–32693
32. Zou, M.-X., Roy A. A. Zhao, Q., Kirshenbaum, L. A., Karmazyn, M., and Chidiac, P. (2006) RGS2 is upregulated by and attenuates the hypertrophic effect of α_1-adrenergic activation in cultured ventricular myocytes. *Cell. Signal.* **18,** 1655–1663
33. Xie, Z., Liu, D., Liu, S., Calderon, L., Zhao, G., Turk, J., and Guo, Z. (2011) Identification of a cAMP-response element in the regulator of G-protein signaling-2 (RGS2) promoter as a key cis-regulatory element for RGS2 transcriptional regulation by angiotensin II in cultured vascular smooth muscles. *J. Biol. Chem.* **286,** 44646–44658
34. Kach, J., Sethakorn, N., and Dulin, N. O. (2012) A finer tuning of G-protein signaling through regulated control of RGS proteins. *Am. J. Physiol. Heart Circ. Physiol.* **303,** H19–H35
35. Bodenstein, J., Sunahara, R. K., and Neubig, R. R. (2007) N-terminal residues control proteasomal degradation of RGS2, RGS4, and RGS5 in human embryonic kidney 293 cells. *Mol. Pharmacol.* **71,** 1040–1050
36. Sjögren, B., Swaney, S., and Neubig, R. R. (2015) FBXO44-mediated degradation of RGS2 protein uniquely depends on a cullin 4B/DDB1 complex. *PLoS One* **10,** e0123581
37. Park, S.-E., Kim, J.-M., Seok, O.-H., Cho, H., Wadas, B., Kim, S.-Y., Varshavsky, A., and Hwang, C.-S. (2015) Control of mammalian G protein signaling by N-terminal acetylation and the N-end rule pathway. *Science* **347,** 1249–1252
38. Sjögren, B., Parra, S., Atkins, K. B., Karaj, B., and Neubig, R. R. (2016) Digoxin-mediated upregulation of RGS2 protein protects against cardiac injury. *J. Pharmacol. Exp. Ther.* **357,** 311–319
39. Sjögren, B., Parra, S., Heath, L. J., Atkins, K. B., Xie, Z.-J., and Neubig, R. R. (2012) Cardiotonic steroids stabilize regulator of G protein signaling 2 protein levels. *Mol. Pharmacol.* **82,** 500–509
40. Raveh, A., Schultz, P. J., Aschermann, L., Carpenter, C., Tamayo-Castillo, G., Cao, S., Clardy, J., Neubig, R. R., Sherman, D. H., and Sjögren, B. (2014) Identification of protein kinase C activation as a novel mechanism for RGS2 protein upregulation through phenotypic screening of natural product extracts. *Mol. Pharmacol.* **86,** 406–416
41. Osei-Owusu, P., Sun, X., Drenan, R. M., Steinberg, T. H., and Blumer, K. J. (2007) Regulation of RGS2 and second messenger signaling in vascular smooth muscle cells by cGMP-dependent protein kinase. *J. Biol. Chem.* **282,** 31656–31665
42. Salim, S., Sinnarajah, S., Kehrl, J. H., and Dessauer, C. W. (2003) Identification of RGS2 and type V adenylyl cyclase interaction sites. *J. Biol. Chem.* **278,** 15842–15849
43. Gu, S., Anton, A., Salim, S., Blumer, K. J., Dessauer, C. W., and Heximer, S. P. (2008) Alternative translation initiation of human regulators of G-protein signaling-2 yields a set of functionally distinct proteins. *Mol. Pharmacol.* **73,** 1–11
44. Noé, L., Di Michele, M., Giets, E., Thys, C., Wittevrongel, C., De Vos, R., Overbergh, L., Waelkens, E., Jaeken, J., Van Geet, C., and Freson, K. (2010) Platelet Gs hypofunction and abnormal morphology resulting from a heterozygous RGS2 mutation. *J. Thromb. Haemost.* **8,** 1594–1603
45. Tasaki, T., Sriram, S. M., Park, K. S., and Kwon, Y. T. (2012) The N-end rule pathway. *Annu. Rev. Biochem.* **81,** 261–289
46. Hahntow, I. N., Mairuhu, G., van Valkengoed, I. G. M., Baas, F., Alewijnse, A. E., Koopmans, R. P., and Michel, M. C. (2009) Are RGS2 gene polymorphisms associated with high blood pressure in an ethnicity- and gender-specific manner? *Am. J. Hypertens.* **22,** 80–86
47. Osei-Owusu, P., Sabharwal, R., Kaltenbronn, K. M., Rhee, M.-H., Chapleau, M. W., Dietrich, H. H., and Blumer, K. J. (2012) Regulator of G protein signaling 2 deficiency causes endothelial dysfunction and impaired endothelium-derived hyperpolarizing factor-mediated relaxation by dysregulating $G_{i/o}$ signaling. *J. Biol. Chem.* **287,** 12541–12549
48. Thestrup, T., Litzlbauer, J., Bartholomäus, I., Mues, M., Russo, L., Dana, H., Kovalchuk, Y., Liang, Y., Kalamakis, G., Laukat, Y., Becker, S., Witte, G., Geiger, A., Allen, T., Rome, L. C., Chen, T.-W., Kim, D. S., Garaschuk, O., Griesinger, C., and Griesbeck, O. (2014) Optimized ratiometric calcium sensors for functional *in vivo* imaging of neurons and T lymphocytes. *Nat. Meth.* **11,** 175–182
49. Heximer, S. P., Lim, H., Bernard, J. L., and Blumer, K. J. (2001) Mechanisms governing subcellular localization and function of human RGS2. *J. Biol. Chem.* **276,** 14195–14203
50. Osei-Owusu, P., Knutsen, R. H., Kozel, B. A., Dietrich, H. H., Blumer, K., and Mecham, R. P. (2014) Altered reactivity of resistance vasculature contributes to hypertension in elastin insufficiency. *Am. J. Physiol. Heart Circ. Physiol.* **306,** H656–H666
51. de Queiroz, D. B., Sastre, E., Caracuel, L., Callejo, M., Xavier, F. E., Blanco-Rivero, J., and Balfagón, G. (2015) Alterations in perivascular innervation function in mesenteric arteries from offspring of diabetic rats. *Br. J. Pharmacol.* **172,** 4699–4713
52. Sastre, E., Blanco-Rivero, J., Caracuel, L., Callejo, M., and Balfagón, G. (2015) Alterations in perivascular sympathetic and nitrergic innervation function induced by late pregnancy in rat mesenteric arteries. *PLoS One* **10,** e0126017
53. Lu, C., Su, L. Y., Lee, R. M. K. W., and Gao, Y. J. (2010) Mechanisms for perivascular adipose tissue-mediated potentiation of vascular contraction

to perivascular neuronal stimulation: The role of adipocyte-derived angiotensin II. *Eur. J. Pharmacol.* **634,** 107–112
54. Johnson, P. R., Swanson, R., Rakhilina, L., and Hochstrasser, M. (1998) Degradation signal masking by heterodimerization of MATα2 and MATa1 blocks their mutual destruction by the ubiquitin-proteasome pathway. *Cell* **94,** 217–227
55. Han, S., Liu, Y., and Chang, A. (2007) Cytoplasmic Hsp70 promotes ubiquitination for endoplasmic reticulum-associated degradation of a misfolded mutant of the yeast plasma membrane ATPase, PMA1. *J. Biol. Chem.* **282,** 26140–26149
56. Sadowski, M., Suryadinata, R., Lai, X., Heierhorst, J., and Sarcevic, B. (2010) Molecular basis for lysine specificity in the yeast ubiquitin-conjugating enzyme Cdc34. *Mol. Cell. Biol.* **30,** 2316–2329
57. David, Y., Ziv, T., Admon, A., and Navon, A. (2010) The E2 ubiquitin-conjugating enzymes direct polyubiquitination to preferred lysines. *J. Biol. Chem.* **285,** 8595–8604
58. Prakash, S., Tian, L., Ratliff, K. S., Lehotzky, R. E., and Matouschek, A. (2004) An unstructured initiation site is required for efficient proteasome-mediated degradation. *Nat. Struct. Mol. Biol.* **11,** 830–837
59. Guharoy, M., Bhowmick, P., Sallam, M., and Tompa, P. (2016) Tripartite degrons confer diversity and specificity on regulated protein degradation in the ubiquitin-proteasome system. *Nat. Commun.* **7,** 10239
60. Jong, Y.-J. I., Kumar, V., Kingston, A. E., Romano, C., and O'Malley, K. L. (2005) Functional metabotropic glutamate receptors on nuclei from brain and primary cultured striatal neurons. Role of transporters in delivering ligand. *J. Biol. Chem.* **280,** 30469–30480

Proteolytic degradation of regulator of G protein signaling 2 facilitates temporal regulation of $G_{q/11}$ signaling and vascular contraction

Stanley M. Kanai, Alethia J. Edwards, Joel G. Rurik, Patrick Osei-Owusu and Kendall J. Blumer

J. Biol. Chem. 2017, 292:19266-19278.
doi: 10.1074/jbc.M117.797134 originally published online October 3, 2017